Contribution from the Department of Macromolecular Science, Faculty of Science, Osaka University, Toyonaka, Osaka 560, Japan

Control of Fe-S Bond Character by the Variation of Fe-S Torsion Angles in the Iron(III) Site of Rubredoxin

Norikazu Ueyama, Takashi Sugawara, Kazuyuki Tatsumi, and Akira Nakamura*

Received September 10, 1986

The spectroscopic and electrochemical study of $[Fe(Z\text{-}cys\text{-}Pro\text{-}Leu\text{-}cys\text{-}OMe)_2]^{-/2-}$ (Z = benzyloxycarbonyl) as a model complex of rubredoxin suggests a conformationally restricted rotation of the Fe-S torsion angle by the Cys-X-Y-Cys chelation. The dependence of Fe-S bond properties on the rotation of Fe-S torsion angles was established by the extended Hückel MO calculations. This explains the observed distortion (C_2) from a D_{2d} structure with the chelating Cys-X-Y-Cys sequence and the resulting change of spectroscopic and magnetic properties.

Introduction

Rubredoxin is known to be an electron-transfer mediator in many biological systems.[1] The active site of rubredoxin has a simple structure with an Fe(II) or Fe(III) ion surrounded by four cysteinyl thiolate (cys-*S*) ligands that are involved in two invariant Cys-X-Y-Cys (X, Y = amino acid residues) sequences. For example, *Clostridium pasteurianum* rubredoxin has Cys(6)-Thr-Val-Cys(9) and Cys(39)-Pro-Leu-Cys(42) sequences around the active site.[2] No significant distortion of the Fe(III) geometry has been discussed, either from the X-ray analysis of rubredoxin by Watenpaugh et al.[3] or from the EXAFS analysis.[4] However, the Raman spectra of the oxidized rubredoxin have suggested an unproved distortion of the $[Fe(cys\text{-}S)_4]^-$ core.[5] Experimentally, the distortion from T_d has been speculated from the splitting of the d-d extrema in the CD spectra of rubredoxin[6] and from the observation of characteristic ligand-metal charge-transfer bands in the MCD spectra of rubredoxin[7] and the model complexes containing Cys-Pro-Leu-Cys or Cys-Ala-Ala-Cys peptides.[8] Appearance of the characteristic bands has been considered to be due to the splitting by an unproved distortion.

The electronic perturbation on Fe(III) by the peptide chain has been discussed, since the redox potentials of native rubredoxins are quite different from those of simple alkanethiolate model complexes.[9] To elucidate the perturbation, we have systematically synthesized Cys-containing peptide model complexes, especially having a Cys-X-Y-Cys sequence that is invariant for many kinds of rubredoxins. We proposed that the chelation of Cys-X-Y-Cys toward the Fe(II) or Fe(III) ion forces the ligand to form a NH---S hydrogen bond even in *N,N*-dimethylformamide, resulting in the positive shift of the redox potential.[10] On the other hand, the thermal stability of the redox couple (2-/1-) depends on the identity of X and Y residues interposed between two Cys residues in $[Fe(Z\text{-}cys\text{-}X\text{-}Y\text{-}cys\text{-}OMe)_2]^{-/2-}$.[11] The hydrophobicity of side chains of the X and Y residues was considered to be crucial for the thermal stability of the Fe(III) state of $[Fe(SR)_4]^-$.[10,12,13]

Table I. Input Parameters for the Structure Calculation of $[Fe(SCH_3)_4]^-$

atoms	length, Å	atoms	angle, deg
Fe-S	2.29	Fe-S-C	109.47
S-C	1.80	S-C-H	109.47
C-H	1.09		

Besides the presence of NH---S hydrogen bonds, a chelation effect of the Cys-X-Y-Cys ligand is proposed for the positive shift of the redox potential and for the stability of the 1- oxidation state in rubredoxin. The chelating effect is mainly associated with the control of Fe-S bond character by a specific orientation of Fe-S-C, as shown in illustration I, which has been suggested by the

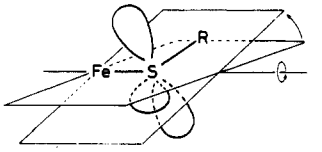

I

CD and MCD studies of a DMF solution of Fe(III)/Z-Cys-X-Y-Cys-OMe (X-Y = Pro-Leu, Ala-Ala) containing the $[Fe(Z\text{-}cys\text{-}X\text{-}Y\text{-}cys\text{-}OMe)_2]^-$ complex.[8] However, no observation of the characteristic MCD band due to such a chelating effect has been reported for $[Fe(S_2\text{-}o\text{-}xyl)_2]^-$ (S_2-*o*-xyl = *o*-xylylene-α,α'-dithiolate) even with its effectively chelating dithiolate ligand.[8,9]

Some theoretical calculations using simple extended Hückel MO calculations for the $[Fe(SR)_4]^{2-/-}$ model have been carried out to estimate the electronic polarization of the Fe-S bond.[14-16] Noodleman et al. have reported the Xα valence-bond scattered-wave calculations for $[Fe(SR)_4]^{-/2-}$ (R = H, CH_3).[17] In this paper, the chelation effect arising from the orientation of Fe-S-C with the variation of Fe-S torsion angles is evaluated by using the extended Hückel molecular orbital calculations.

Method of Extended Hückel Calculations

For approximation of the Fe(III) site in the active site of rubredoxin, a D_{2d} structure for $[Fe(S\text{-}CH_3)_4]^-$ can be given with a tetrahedral structure of the FeS_4 core. the D_{2d} symmetry is considered to be the most stable structure in $[Fe(SR)_4]^{-/2-}$. Actually, the crystal structure of $[PPh_4]_2[Fe(SPh)_4]$ determined by X-ray analysis has been reported to have a D_{2d} structure.[18] The assumed geometry used for the calculation is illustrated in Figure 1a. The parameters employed are listed in Table I. $[Fe(Z\text{-}cys\text{-}Ala\text{-}Ala\text{-}cys\text{-}OMe)_2]^-$, with two Cys-X-Y-Cys sequences, has a C_2 symmetry with a slight variation of the two Fe-S torsion angles, which is illustrated in Figure 1b. The two Cys-X-Y-Cys sequences in the active site of *C. pasteurianum* rubredoxin have approximately the same geometry.[3] The extended Hückel parameters for Fe(III) were cited from

(1) Lode, E. T.; Coon, M. J. *Iron-Sulfur Proteins*; Lovenberg, W., Ed.; Academic: New York, 1973; Vol. I, pp 173-191.
(2) Orme-Johnson, W. *Annu. Rev. Biochem.* **1973**, *42*, 159.
(3) Watenpaugh, K. D.; Sieker, L. C.; Jensen, L. H. *J. Mol. Biol.* **1979**, *131*, 509.
(4) Shulman, R. G.; Eigenberger, P.; Blumberg, W. E.; Stombaugh, N. A. *Proc. Natl. Acad. Sci. U.S.A.* **1975**, *72*, 4003.
(5) Yachandra, V. K.; Hare, J.; Moura, I.; Spiro, T. G. *J. Am. Chem. Soc.* **1983**, *105*, 6455.
(6) Eaton, W. A.; Lovenberg, W. *Iron-Sulfur-Proteins*; Lovenberg, W., Ed.; Academic: New York, 1973; Vol. II, pp 131-162.
(7) Ulmer, D. D.; Holmquist, B.; Valee, B. L. *Biochem. Biophys. Res. Commun.* **1973**, *51*, 1054.
(8) Nakata, M.; Ueyama, N.; Nakamura, A. *Bull. Chem. Soc. Jpn.* **1983**, *56*, 3647.
(9) Lane, R. W.; Ibers, J. A.; Frankel, R. B.; Holm, R. H. *Proc. Natl. Acad. Sci. U.S.A.* **1975**, *72*, 2868.
(10) Ueyama, N.; Nakata, M.; Fuji, M.; Terakawa, T.; Nakamura, A. *Inorg. Chem.* **1985**, *24*, 2190.
(11) Lower-case cys refers to a Cys residue involved in coordination.
(12) Ueyama, N.; Nakata, M.; Nakamura, A. *Bull. Chem. Soc. Jpn.* **1981**, *54*, 1727.
(13) Millar, M.; Lee, J. F.; Koch, S. A.; Fikar, R. *Inorg. Chem.* **1982**, *21*, 4106.
(14) Loew, G. H.; Chadwick, M.; Steinberg, D. A. *Theor. Chim. Acta* **1974**, *33*, 125.
(15) Loew, G. H.; Lo, D. Y. *Theor. Chim. Acta* **1974**, *32*, 217.
(16) Loew, G. H.; Chadwick, M.; Lo, D. Y. *Theor. Chim. Acta* **1974**, *33*, 147.
(17) Noodleman, L.; Norman, J. G., Jr.; Osborne, J. H.; Aizman, A.; Case, D. A. *J. Am. Chem. Soc.* **1985**, *107*, 3418.
(18) Coucouvanis, D.; Swenson, D.; Baenziger, N. C.; Murphy, C.; Holah, D. G.; Sfarnas, N.; Simopoulos, A.; Kostikas, A. *J. Am. Chem. Soc.* **1981**, *103*, 3350.

0020-1669/87/1326-1978$01.50/0

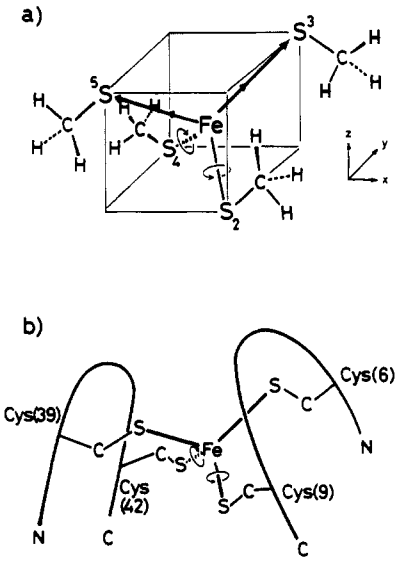

Figure 1. (a) Schematic geometry of the $[Fe(SCH_3)_4]^-$ model used for the calculation. (b) Schematic presentation of the proposed structure for $[Fe(Z\text{-cys-X-Y-cys-OMe})_2]^-$ or native rubredoxin.

the earlier work.[19] The standard parameters for S, C, and H were employed. The high-spin configuration of the five Fe(iII) d electrons was assumed for the Mo calculations.

Results and Discussion

Chelation Effect and NH---S Hydrogen Bonding of Cys-X-Y-Cys. In our previous spectral study on various Fe(III) complexes of Cys-containing peptides,[12] the MCD spectra of $[Fe(Z\text{-cys-Pro-Leu-cys-OMe})_2]^-$ and $[Fe(Z\text{-cys-Ala-Ala-cys-OMe})_2]^-$ showed a negative Faraday *B* term at about 28 600 cm^{-1} similar to that (28 800 cm^{-1}) of *C. pasteurianum* rubredoxin. The 28 200–28 600-cm^{-1} band assignable to a ligand–metal charge transfer has been reported to be due to the transition of the highest occupied ligand $p\pi$ (nonbonding orbitals) to the half-occupied Fe(III) d orbitals.[20] However, the Fe(III) complex of Z-Ala-Cys-OMe or S_2-*o*-xyl has no such a band at 35 000–25 000 cm^{-1}. Only the Fe(III) complexes of the chelating peptides, Z-Cys-X-Y-Cys-OMe, showed such a characteristic band at 28 200–28 800 cm^{-1}. The MCD spectral characteristics sensitively reflect the variation of Fe–S bond properties by the orientation of S $p\pi$ orbitals of the Cys thiolate toward the Fe(III) d orbitals. thus, the orientation is obviously induced by the Cys-X-Y-Cys chelation.

The chelation ability of Cys-X-Y-Cys to the Pd(II) ion has been studied systematically.[21] Z-Cys-Ala-Ala-Cys-OMe is the most suitable ligand for the chelation to a square-planar Pd(II) ion, whereas Z-Cys-Val-Val-Cys-OMe has almost no ability for the chelation, giving a polymeric structure.

Recently, we found that the Cys-X-Y-Cys sequence chelates to one Fe(III) ion with two Cys thiolates of $[Fe_2S_2(Z\text{-cys-X-Y-cys-OMe})_2]^{2-}$ (X-Y = Ala-Ala, Pro-Leu) complexes. Many of the Z-Cys-X-Y-Cys-OMe peptides except for Z-Cys-Val-Val-Cys-OMe were found to chelate only one Fe(III) ion without bridging between two Fe(III) ions in the $[Fe_2S_2]^{2+}$ core.[22,23] The ^1H NMR spectrum of $[Fe_2S_2(Z\text{-cys-Ala-Ala-cys-OMe})_2]^{2-}$ exhibited two Cys CH_2 peaks at 30.7 and 22.9 ppm in Me_2SO-d_6, which is contact-shifted due to the spin delocalization through the Fe–S–C bond. The 2Fe-2S complex of Z-Cys-Ala-OMe or Z-Ala-Cys-OMe exhibits only one peak at approximately 31 ppm in Me_2SO-d_6. The chelation forces the tetrapeptides to form a NH---S hydrogen bond between the second Ala NH and the second Cys thiolate of the chelation even in a strongly solvating solvent, e.g., Me_2SO-d_6. The NH---S hydrogen bond changes the degree of the contact shift in the ^1H NMR spectrum of $[Fe_2S_2(cys\text{-peptide})_4]^{2-}$. The chelating peptide provides two clearly separated proton signals assignable to Cys CH_2. $[Fe_2S_2(Z\text{-cys-Ala-Pro-cys-OMe})_2]^{2-}$ exhibits two distinct peaks at 34.5 and 31.3 ppm in Me_2SO-d_6 despite less contribution from the NH---S hydrogen bonds.

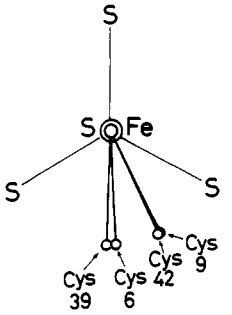

Figure 2. Torsion angles of Fe–S bonds for *C. pasteurianum* native rubredoxin reported by Watenpaugh et al.[22,23]

The results suggest that the chelation of Cys(1)-X-Y-Cys(4) to the Fe(III) ion gives two different types of Fe–S bonds, with or without a NH---S hydrogen bond. The chelating effect is ascribed to the conformationally restricted rotation of the Fe–S torsion angles induced by the bulky side chains of the X and Y residues, since the Fe–S bond properties probably depend on π-interaction between Fe(III) and S $p\pi$ orbitals. Either the Cys(1) Fe–S bond or the Cys(4) Fe–S bond has a different bond character resulting from the different orientation of Fe–S–C. In the case of the rubredoxin model complexes, this has been suggested by our previous MCD spectral results for $[Fe(Z\text{-cys-X-Y-cys-OMe})_2]^-$, as mentioned above. Thus, besides NH---S hydrogen bonds, the restricted orientation of Fe–S–C by the chelation plays a significant role in the control of Fe–S bond characters.

Fe–S Torsion Angle Dependence of Fe–S Bond Character. In general, a staggered state for the Fe–S torsion angle is stable for steric reasons. Therefore, a staggered Fe–S torsion angle of the D_{2d} structure can be defined with $\psi = 0°$. In the case of the Fe complex of Cys(1)-X-Y-Cys(4), the rotation of the Fe–S torsion angle induced conformationally by the chelation effect appears at the position of the former Cys(1) or the latter Cys(4). Two *eclipsed* Fe–S torsion angles ($\psi = +30°$) can be found in the active site of *C. pasteurianum* rubredoxin.[24] Figure 2 is drawn on the basis of the parameters of the X-ray analysis by Watenpaugh et al.,[3,24] which were obtained from the Protein Data Bank.[25] The Fe–S torsion angles of the two Cys(4) residues are observed with a change from the staggered position to an eclipsed position in the two Cys(1)-X-Y-Cys(4) sequences of *C. pasteurianum* rubredoxin.

The torsion angle dependence of the Fe–S bond properties was examined by the extended Hückel MO calculations on a model complex, $[Fe(SCH_3)_4]^{1-/2-}$ (D_{2d}) as shown in Figure 1a. The two Fe–S torsion angles in two Cys-X-Y-Cys sequences of native protein correspond to the deviated torsion angles of Fe_1–S_2 and Fe_1–S_4 in the same direction (Figure 1b), and the other two torsion angles of Fe_1–S_3 and Fe_1–S_5 were fixed at $\psi = 0°$ in the staggered position. Then, the geometry alters a C_2 symmetry from D_{2d}. Figure 3 shows the overlap populations for Fe–S bonds by variation of the Fe_1–S_2 and Fe_1–S_4 torsion angles. The results of the calculations suggest the distinguishable dependence of the Fe–S overlap populations upon variation of the Fe–S torsion angles.

In the case of the Fe(III) site of *C. pasteurianum* rubredoxin, Cys(9) and Cys(42) residues are skewed about $\psi = +30°$ as an eclipsed position in Figure 2. The overlap populations for Cys(9) and Cys(42) residues were estimated to be 0.532, whereas the

(19) Tatsumi, K.; Hoffmann, R. *J. Am. Chem. Soc.* **1981**, *103*, 3328.
(20) Bair, R. A.; Goddard, W. A., III *J. Am. Chem. Soc.* **1978**, *100*, 5669.
(21) Ueyama, N.; Nakata, M.; Nakamura, A. *Inorg. Chim. Acta* **1981**, *55*, L61.
(22) Ueno, S.; Ueyama, N.; Nakamura, A.; Tsukihara, T. *Inorg. Chem.* **1986**, *25*, 1000.
(23) Ueyama, N.; Ueno, S.; Nakamura, A. *Bull. Chem. Soc. Jpn.* **1987**, *60*, 283.
(24) Watenpaugh, K. D.; Sieker, L. C.; Jensen, L. H. *J. Mol. Biol.* **1980**, *138*, 615.
(25) Taketani, M.; Iga, Y.; Matsuura, Y.; Yasuoka, N.; Kakudo, M.; Isomoto, Y. *Proc. Int. CODATA Conf.* **1980**, *7*, 84.

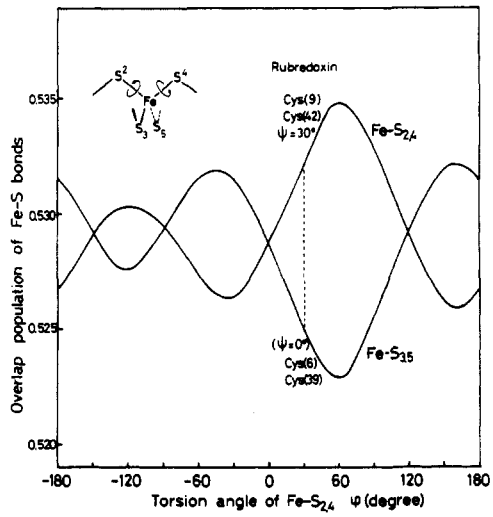

Figure 3. Variation of the overlap population of Fe–S bonds depending on the Fe–S torsion angles (four Fe–S bond lengths are fixed).

Table II. Fe–S Bond Lengths and Fe–S–C Bond Angles in *C. pasteurianum* Rubredoxin Reported by Watenpaugh et al.[3]

	1.2-Å resolution	
residues	Fe–S, Å	Fe–S–C, deg
Cys(6)	2.239	100.70
Cys(9)	2.287	109.22
Cys(39)	2.308	99.98
Cys(42)	2.251	111.50

overlap populations for the staggered Cys(6) and Cys(39) residues were found to be 0.525. The larger Fe–S overlap populations for Cys(9) and Cys(42) residues indicate that the Fe–S bonds become stronger with π-bonding interaction, since the increase of the overlap populations corresponds to the increase of the π-bonding character. The larger Fe–S overlap population is reflected by shortening of two Fe–S bond lengths in the X-ray data. On the contrary, the Fe–S bonds of the nonskewed Cys(6) and Cys(39) residues are weaker with less π-bonding character. this is reflected by elongation of the Fe–S bond lengths for the Cys(6) and Cys(39) residues.

The results of the theoretical calculations are consistent with the experimental results for the Fe–S bond lengths of the 1.2-Å X-ray analysis of *C. pasteurianum* rubredoxin by Watenpaugh et al. (Table II).[3,24] The Fe–S lengths of the eclipsed Cys(9) and Cys(42) residues are reported to be 2.235–2.288 Å, while those of the staggered Cys(6) and Cys(39) residues are 2.308–2.333 Å. In this case, the comparison of the Fe–S bond lengths is available with a smaller standard deviation than those from the EXAFS study.

The Fe–S–C angles of the active site of *C. pasteurianum* rubredoxin provide more unambiguous evidence for the distortion as cited in Table II. These Fe–S–C angles can be classified into two groups, which correspond to two groups of the Fe–S bond distances. Two thiolate ligands have large Fe–S–C angles (108–111°) associated with the shorter Fe–S distances. The two other thiolate ligands have smaller Fe–S–C angles (99–101°). In general, the strong M–S bonds of $[M(SR)_4]^{n-}$, e.g. $[M(SPh)_4]^{2-}$ (M = Zn(II), Cd(II), Ni(II), Co(II), Mn(II)),[26] and the strong Cu–S bond of the active site of plastocyanin,[27] have large M–S–C angles (107–110°), with the larger π-interaction between M^{n+} and S. On the contrary, a smaller S–S–C angle (103–104°), which is caused by the single-bond character of S–S, has been reported for Ph–S–S–Ph and Bzl–S–S–Bzl.[28] Lane et al. have reported

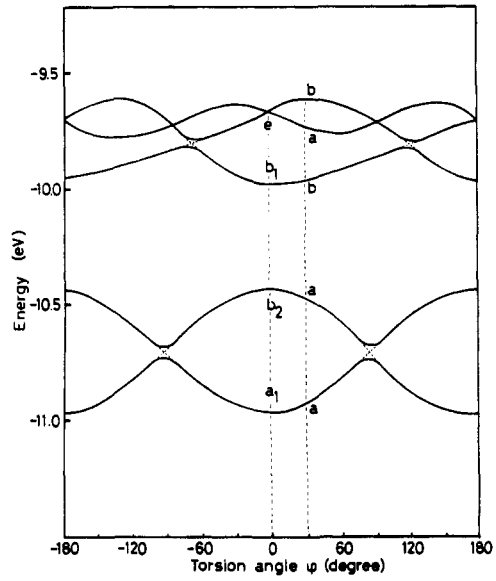

Figure 4. Variation of energy levels with the change of the Fe–S torsion angles.

a small mean value (101.5°) for the four Fe–S–C angles of $[Fe(S_2\text{-}o\text{-}xyl)_2]^-$,[24] but unfortunately it is not reasonable to compare it with the above M–S–C values because of the extremely restricted chelating ligand.

The energy levels of Fe 3d orbitals for $[Fe(SCH_3)_4]^-$ are illustrated in Figure 4. The electron configuration was assumed with five half-filled molecular orbitals. The splitting of the degenerate e orbitals is explicable by a C_2 structure with two eclipsed Fe–S torsion angles (ψ = +30°). The oxidized forms of rubredoxin and its model complexes, $[Fe(Z\text{-cys-Pro-Leu-cys-OMe})_2]^-$ or $[Fe(Z\text{-cys-Ala-Ala-cys-OMe})_2]^-$, exhibit a characteristic MCD absorption at 28 600–28 800 cm^{-1}. This transition was originally assigned to S (p_x, p_y) → $d_{x^2-y^2}$ at ψ = 0°, which is mixed with d_{z^2} at ψ = +30°. The mixing leads to π-interaction between p_z and d_{z^2} with a S (p_x, p_y, p_z) → $d_{x^2-y^2}$ + d_{z^2} LMCT transition for the eclipsed Fe–S bond, whereas no S p_z interaction is involved with $d_{x^2-y^2}$ + d_{z^2} for the staggered Fe–S bond. This LMCT transition, which was observed as a characteristic MCD extremum, is caused by the eclipsed Fe–S torsion angle (C_2). This splitting also contributes to the appearance of the CD extrema at 6000 and 7400 cm^{-1} due to d–d transitions that have been reported by Eaton and Lovenberg.[6]

Consequently, these LMCT MCD bands and d–d CD bands are ascribed to the eclipsed Fe–S torsion angle (C_2), which was induced by Cys-X-Y-Cys sequences. It is surprising that the Cys-X-Y-Cys sequence can provide a crucial change of Fe–S bond properties with only a slight variation of the Fe–S torsion angle as shown in Figure 3. It is certain that even a local part of the protein, Cys-X-Y-Cys, controls predominantly most of the chemical properties.

Contribution of Chelating Peptides to the Redox Character. The importance of Fe(II) or Fe(III) bound by the peptide chain has been discussed in terms of fine-tuning the electrochemical properties in biological systems. We have examined the role of a local peptide fragment, such as the invariant sequence Cys-X-Y-Cys, around the active site of rubredoxin. Two amino acid residues (X and Y) intervening between two Cys residues also play a significant role in the control of redox properties. For example, the peptide model complexes for reduced rubredoxin, $[Fe(Z\text{-cys-Pro-Leu-cys-OMe})_2]^{2-}$ and $[Fe(Z\text{-cys-Ala-Ala-cys-OMe})_2]^{2-}$, show a quite stable 2−/1− redox couple in Me_2SO, but not $[Fe(Z\text{-cys-Thr-Val-cys-OMe})_2]^{2-}$.

Native rubredoxin has an Fe(II)/Fe(III) redox couple at −0.31 V vs. SCE.[29] Simple alkanethiolate complexes exhibit a more negative redox potential in organic solvents, e.g., −0.99 V vs. SCE

(26) Swenson, D.; Baenziger, N. C.; Coucouvanis, D. *J. Am. Chem. Soc.* **1978**, *100*, 1932.
(27) Penfield, K. W.; Gay, R. R.; Himmelwright, R. S.; Eickman, N. C.; Norris, V. A.; Freeman, H. C.; Solomon, E. I. *J. Am. Chem. Soc.* **1981**, *103*, 4382.
(28) Van Wart, H. E.; Scheraga, H. A. *J. Phys. Chem.* **1976**, *80*, 1812.
(29) Adman, E. T. *Biochem. Biophys. Acta* **1979**, *549*, 107.

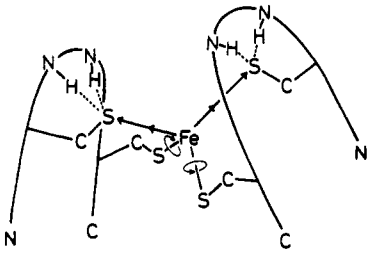

Figure 5. Chelating effects of Cys-X-Y-Cys sequences with NH---S hydrogen bonding and restricted rotation of the Fe–S torsion angles.

for $[Fe(S_2\text{-}o\text{-}xyl)_2]^{2-}$ in Me_2SO. The Fe(II) complexes of Cys-X-Y-Cys peptides showed remarkably shifted redox potentials in Me_2SO. For example, $[Fe(Z\text{-}cys\text{-}Pro\text{-}Leu\text{-}cys\text{-}OMe)_2]^{2-}$ has a 2−/1− couple at −0.5 V vs. SCE. One of the important factors of the positive shift has been proposed to be a NH---S hydrogen bond that forms between Cys(1) S and Cys(4) NH or Y NH groups of the chelating Cys(1)-X-Y-Cys(4) ligand, as shown in Figure 5. Elongation of the Fe–S bond with the NH---S hydrogen bond and the chelation effect provide for conditions that give ionic character to the Fe–S bond. In general, an Fe(III) ion with four thiolato ligands, such as $[Fe(SR)_4]^-$, is thermodynamically unstable and is readily decomposed by dissociation of the ligand (RS^- or $RS^\bullet$). However, native rubredoxin is stable with Fe at this oxidized state (Fe(III). Another important factor for the shift can be proposed: the distortion around Fe(III) by the variation of Fe–S torsion angles in a chelating Cys-X-Y-Cys.

In conclusion, the conformational restriction of the Cys-X-Y-Cys chelating peptides in rubredoxin and its peptide model complexes induces a C_2 distortion around Fe(III). The distortion can successfully explain the characteristic CD and MCD extrema. Further work is under way to investigate the contributions of the distortion to thermodynamic stability and electrochemical properties.

Contribution from the Department of Chemistry,
University of Texas at El Paso, El Paso, Texas 79968-0513

Dissociation Kinetics of 1,10-Diaza-4,7,13,16-tetraoxacyclooctadecane-*N*,*N*′-diacetic Acid Complexes of Lanthanides

C. Allen Chang* and V. Chandra Sekhar

Received August 19, 1986

The dissociation kinetics of 1,10-diaza-4,7,13,16-tetraoxacyclooctadecane-*N*,*N*′-diacetic acid (K22DA) complexes of lanthanide(III) ions were studied in perchloric acid and other media, over the concentration range 5×10^{-4} to 7.5×10^{-3} M and at a constant ionic strength of 0.1 M ($LiClO_4$). Copper(II) was used as the scavenger of free ligand, and the rates of dissociation of these complexes have been found to be independent of $[Cu^{2+}]$. All the complexes exhibit acid-dependent and acid-independent pathways in a manner similar to those of $LnCyDTA^-$ complexes (CyDTA = *trans*-1,2-diaminocyclohexane-*N*,*N*,*N*′,*N*′-tetraacetate ion). Unlike lanthanide (Ln) complexes of 1,7-diaza-4,10,13-trioxacyclopentadecane-*N*,*N*′-diacetic acid (K21DA), $LnK22DA^+$ complex dissociation rates are independent of [anion] and [electrolyte]. There is also no general-acid catalysis. The overall results are compared with those of complexes that are structural analogues such as $LnK21DA^+$, LnMEDTA (MEDTA = *N*-methylethylenediamine-*N*,*N*,*N*′-triacetate ion), and $LnCyDTA^-$. A rationalization is given to account for similarities and differences with respect to observed kinetic characteristics. A number of postulates concerning the relationship between thermodynamic and kinetic stabilities and the detailed reaction mechanisms of lanthanide complexes of polyamino polyacetate ligands are proposed.

The study of solution thermodynamic complex formation and kinetic (both formation and dissociation) stabilities of lanthanide complexes have been of interest for a number of years because of their significant implications in analytical, biological, and other chemical applications.[1-7] In general, it is observed that the ligand topology can affect the thermodynamic and kinetic stabilities of lanthanide complexes. Ligand characteristics such as the charge, cavity size, number of donor atoms, and stereochemical constraints imposed are all found to be important. Thus, it is believed that by varying these factors, one might be able to develop ion selective reagents for an individual or a group of metal ions.

In order to develop lanthanide ion selective reagents, we have initiated a systematic study of lanthanide complexes of two macrocyclic compounds with ionizable pendant functional groups, i.e., 1,7-diaza-4,10,13-trioxacyclopentadecane-*N*,*N*′-diacetic acid (DAPDA or K21DA) and 1,10-diaza-4,7,13,16-tetraoxacyclooctadecane-*N*,*N*′-diacetic acid (DACDA or K22DA) (Figure 1). The stability constants of lanthanide complexes of the two ligands have been previously reported.[8,9] Also, for the reason of convenience of study by a stopped-flow spectrophotometer, we have studied the dissociation kinetics of K21DA complexes of lanthanides.[10] The dissociation reaction rates together with the stability constants allow the calculation of formation rate constants, which may otherwise be difficult to obtain experimentally. Both formation and dissociation kinetic studies can afford further information concerning mechanistic details.

For lanthanide complexes of multidentate ligands such as polyamino polycarboxylic acids, the dissociation reactions show strong pH dependence with the rate and mechanism changing upon changes in acid strength. Two types of pH dependence have been observed, a linear dependence and a saturation kinetic dependence. Examples of the latter include those complexes of *N*-methyl-

(1) Moeller, T.; Martin, D. F.; Thompson, L. C.; Ferrus, R.; Feistel, G. R.; Randall, W. J. *Chem. Rev.* **1965**, *65*, 1.
(2) Bünzli, J.-C. G.; Wessner, D. *Coord. Chem. Rev.* **1984**, *60*, 191–253.
(3) Thompson, L. C.; Loraas, J. A. *Inorg. Chem.* **1962**, *1*, 490; **1963**, *2*, 89.
(4) Purdie, N.; Farrow, M. M. *Coord. Chem. Rev.* **1973**, *11*, 189–226.
(5) Brucher, E.; Banyai, I. *J. Inorg. Nucl. Chem.* **1980**, *42*, 749–756.
(6) Southwood-Jones, R. V.; Merback, A. E. *Inorg. Chim. Acta* **1978**, *30*, 77; *Ibid.* **1978**, *30*, 135.
(7) Glentworth, P.; Wiseall, B.; Wright, C. L.; Mahmood, A. J. *J. Inorg. Nucl. Chem.* **1968**, *30*, 967–986.
(8) Chang, C. A.; Rowland, M. E. *Inorg. Chem.* **1983**, *22*, 3866–3869.
(9) Chang, C. A.; Ochaya, V. O. *Inorg. Chem.* **1986**, *25*, 355–358.
(10) Sekhar, V. C.; Chang, C. A. *Inorg. Chem.* **1986**, *25*, 2061–2065.

0020-1669/87/1326-1981$01.50/0